ECCOMAS Congress 2016
VII European Congress on Computational Methods in Applied Sciences and Engineering
M. Papadrakakis, V. Papadopoulos, G. Stefanou, V. Plevris (eds.)
Crete Island, Greece, 5–10 June 2016

REDUCED ORDER MODELLING OF GUST ANALYSIS USING COMPUTATIONAL FLUID DYNAMICS

R. Thormann[1], P. Bekemeyer[2] and S. Timme[3]

[1]Research Associate
University of Liverpool
e-mail: reik.thormann@liverpool.ac.uk

[2]Ph.D. Student and [3]Lecturer
University of Liverpool
e-mail: {philipp.bekemeyer, sebastian.timme}@liverpool.ac.uk

Keywords: Reduced Order Modelling, Gust Response, Computational Fluid Dynamics, Reynolds-averaged Navier-Stokes Equations

Abstract. *The simulation of gust responses is a crucial task in the design and certification process of a new aircraft. Moreover, if high accuracy is desired, the computational cost can be overwhelming. Linear frequency-domain methods have previously shown significant reduction in computational cost for motion-induced aerodynamics as well as for gust excitations. Time-domain signals are reconstructed by a superposition of responses at several discrete frequencies. Rather than using the frequency-domain method directly, a reduced order model is constructed projecting the time-depending linearised Reynolds-averaged Navier-Stokes equations on a basis obtained by proper orthogonal decomposition. The resulting small-sized ordinary differential equations for the modal coefficients are integrated in time. Results are presented for a two-dimensional NACA 0012 aerofoil covering sub- and transonic conditions including a case with shock-induced separation. Responses due to 1-cos as well as to sharp-edged gusts are compared between the reduced order model and its non-linear full order counterpart showing time histories of the lift coefficient and worst case surface pressure coefficients.*

1 Introduction

Gust load analysis is a key task during design and certification of new aircraft. Simulations have to be performed for a huge number of parameter combinations varying e.g. Mach number, altitude, load factor and gust length. The industrial process currently relies on linear potential methods, such as doublet lattice, which are commonly corrected by quasi-steady data either obtained from wind-tunnel experiments or computational fluid dynamics (CFD) simulations. Since corrections are commonly introduced only at zero frequency, deviations occur at higher frequencies important for shorter gust lengths and unsteady transonic effects – such as resonance behaviour and inverse shock motion – and cannot be captured accurately [1]. Additionally, this approach requires a mapping between the surface representations of the different methods which can become complicated for industrial cases.

In the past few years CFD aerodynamics alone have been used to investigate gust encounter. Examples from simple aerofoils to civil aircraft are available [2, 3, 4]. However, solving the non-linear Reynolds-averaged Navier-Stokes (RANS) equations in the time domain is too time-consuming to cover the complete flight envelope. Reduced order modelling is one alternative to overcome high computational cost. Several approaches are possible to achieve a reduced order model (ROM) for gust interactions including autoregressive methods [3] and eigenvalue realisation [5]. Another model reduction technique is based on proper orthogonal decomposition (POD) [6], which was, with respect to fluid dynamics, first introduced to model coherent structures in turbulent flow fields [7]. Snapshots are computed with the full order method covering the parameter space of interest and a small eigenvalue problem is solved subsequently to obtain a reduced linear basis. The idea of POD using frequency domain sample data was first introduced for the investigation of a simple twelve-degrees-of-freedom mass-spring-damper system combined with an incompressible three-dimensional vortex lattice method [8].

Linearised frequency domain (LFD) methods have also proven to retain the RANS accuracy at significantly reduced computational cost for forced motion simulations [9]. The RANS equations are linearised around a steady state and then solved in the frequency-domain. Moreover, this method was combined with the POD technique for a pitch-plunge aerofoil [10]. An extension to three-dimensional cases, generating snapshots for all structural modes of interest, has also been presented [11]. Recently, this approach was extended towards gust responses and a ROM is presented [12]. The LFD method is first used to generate snapshots of sinusoidal gusts while varying the reduced frequency. Afterwards, a reduced basis is computed using the POD approach and the linearised RANS equations are projected onto the subspace resulting in a small linear system per gust frequency.

In this paper, the approach is modified to solve the projected equations in the time domain to simulate non-periodic excitation, such as 1-cos and sharp-edged gusts more efficiently. Moreover, a time-domain ROM offers the additional advantage to couple the system with a controller for gust load allevation. Viscous results are shown for the NACA0012 aerofoil including non-linearities such as transonic shock waves and boundary layer separation. Responses are compared between the reduced order model and its non-linear full order counterpart showing time histories of the lift coefficient and worst case surface pressure coefficients.

2 Methods

The RANS equations in semi-discrete form read:

$$\frac{\mathrm{d}\mathbf{W}}{\mathrm{d}t}(t) = \mathbf{R}(\mathbf{W}(t), \mathbf{v}_g(t)) \tag{1}$$

with $\mathbf{W}$ denoting the vector of fluid unknowns, $\mathbf{v}_g$ the external excitation due to a gust encounter and $\mathbf{R}$ the non-linear residual function. Separating the variables into a steady and a time-dependent part:

$$\mathbf{W}(t) = \overline{\mathbf{W}} + \widetilde{\mathbf{W}}(t)$$

and expanding eq. (1) around this steady state in a Taylor series yields:

$$\frac{\mathrm{d}\widetilde{\mathbf{W}}}{\mathrm{d}t}(t) = \mathbf{R}(\overline{\mathbf{W}}, 0) + \frac{\partial \mathbf{R}}{\partial \mathbf{W}}\,\widetilde{\mathbf{W}}(t) + \frac{\partial \mathbf{R}}{\partial \mathbf{v}_g}\,\widetilde{\mathbf{v}}_g(t) + \text{H.O.T.}$$

Since $\overline{\mathbf{W}}$ is the steady state, $\mathbf{R}(\overline{\mathbf{W}}, 0)$ is very small and can be omitted. The linear equation for the perturbations is obtained by neglecting all non-linear terms:

$$\frac{\mathrm{d}\widetilde{\mathbf{W}}}{\mathrm{d}t}(t) = \frac{\partial \mathbf{R}}{\partial \mathbf{W}}\,\widetilde{\mathbf{W}}(t) + \frac{\partial \mathbf{R}}{\partial \mathbf{v}_g}\,\widetilde{\mathbf{v}}_g(t) \tag{2}$$

Assuming a harmonic excitation at frequency ω, eq. (2) can be transferred into the frequency domain, yielding the governing equations for the LFD method:

$$\left[\frac{\partial \mathbf{R}}{\partial \mathbf{W}} - j\omega\underline{\mathbf{I}}\right]\widehat{\mathbf{W}} = -\frac{\partial \mathbf{R}}{\partial \mathbf{v}_g}\,\widehat{\mathbf{v}}_g \tag{3}$$

Thus a huge, but sparse system of linear equations is obtained relating the Fourier coefficient of the gust excitation $\widehat{\mathbf{v}}_g$ to the Fourier coefficient of the fluid unknowns $\widehat{\widetilde{\mathbf{W}}}$. The right-hand side vector is computed applying the chain rule:

$$\frac{\partial \mathbf{R}}{\partial \mathbf{v}_g}\,\widehat{\mathbf{v}}_g = \frac{\partial \mathbf{R}}{\partial \dot{\mathbf{x}}}\,\frac{\partial \dot{\mathbf{x}}}{\partial \mathbf{v}_g}\,\widehat{\mathbf{v}}_g$$

where $\dot{\mathbf{x}}$ is the vector of mesh velocities since the gust is simulated applying the field velocity method [13]. The equation can be further simplified by the simple relation $\dot{\mathbf{x}} = -\widehat{\mathbf{v}}_g$. As for the LFD method for forced motion, the fluid Jacobian matrix $\frac{\partial \mathbf{R}}{\partial \mathbf{W}}$ is computed analytically, while the influence of the grid velocities in term $\frac{\partial \mathbf{R}}{\partial \dot{\mathbf{x}}}$ is computed using central finite differences. The complex-valued vector $\widehat{\mathbf{v}}_g$ can be calculated by the analytical expression

$$\widehat{\mathbf{v}}_g(\mathbf{x}, \omega) = v_{gz} e^{j\omega(\mathbf{x}-\mathbf{x}_0)}$$

with v_{gz} denoting the gust amplitude, $\mathbf{x}$ the grid coordinate and $\mathbf{x}_0$ a reference point. The frequency of excitation is defined by

$$\omega = U_\infty \frac{2\pi}{L_g}$$

with L_g as the gust length and U_∞ as the freestream velocity.

2.1 Proper Orthogonal Decomposition

Snapshots are generated at discrete frequencies with sinusoidal excitation solving the linearised frequency-domain system given in eq. (3). Solutions $\widehat{\mathbf{W}}_k$ are stored as columns in the snapshot matrix $\underline{\mathbf{S}}$. The POD basis $\underline{\mathbf{\Phi}}$ is obtained as a linear combination of snapshots

$$\underline{\mathbf{\Phi}} = \underline{\mathbf{S}}\boldsymbol{\nu}_k \tag{4}$$

where the vector $\boldsymbol{\nu}_k$ is scaled so that vectors in $\underline{\mathbf{\Phi}}$ are unit length. The eigenvalue problem

$$\underline{\mathbf{S}}^H\underline{\mathbf{S}}\boldsymbol{\nu}_k = \lambda_k\boldsymbol{\nu}_k, \tag{5}$$

with $\underline{\mathbf{S}}^H\underline{\mathbf{S}}$ a symmetric, positive definite matrix, is solved to ensure the best possible approximation in eq. (4). The relative information content a certain mode λ_k contributes to the system, also often referred to as energy, is given by

$$r_k = \lambda_k \left(\sum_i \lambda_i \right)^{-1} \tag{6}$$

and can be used to decrease the number of modes further by only considering those with a high relative information content.

In order to use the POD basis also for a time-domain ROM the POD basis can either be enhanced by its complex-conjugate or alternatively the complex-conjugate snapshots are included before calculating the POD basis. The time-dependent expression for the perturbations in eq. (2) can be reduced to an ordinary differential equation with the number of degrees of freedom corresponding to the POD subspace:

$$\frac{\mathrm{d}\widetilde{\mathbf{q}}}{\mathrm{d}t}(t) = \underline{\mathbf{\Phi}}^H \frac{\partial \mathbf{R}}{\partial \mathbf{W}} \underline{\mathbf{\Phi}}\widetilde{\mathbf{q}}(t) + \underline{\mathbf{\Phi}}^H \frac{\partial \mathbf{R}}{\partial \dot{\mathbf{x}}} \widetilde{\mathbf{v}}_g(t). \tag{7}$$

with $\widetilde{\mathbf{q}}$ denoting the POD or modal coefficients used to reconstruct the flow solution as

$$\widetilde{\mathbf{W}} = \underline{\mathbf{\Phi}}\,\widetilde{\mathbf{q}}.$$

A backward Euler scheme combined with Newton's method is used to integrate eq. (7) in time. The small-sized differential equation is stiff and an explicit time integration scheme was thus unstable for suitable time step sizes.

The same basis can be used to project the LFD system in eq. (3) onto the POD subspace as shown in [12]. However, there are two advantages of the time-domain ROM over the frequency-domain method. First, maximum loads cannot be computed within the frequency-domain and an additional inverse Fourier transformation has to be performed to reconstruct the flow field. Secondly, the magnitudes at high frequencies for a 1-cos gust excitation are negligibly small as seen in Figure 1(b). Therefore, the responses of a limited number of sinusoidal gust can be computed with a frequency-domain ROM and superposed according to their participation on a 1-cos gust. High freqencies cannot be neglected if a sharp-edged gust is considered on the other hand. A frequency-domain ROM must compute the response for all Fourier coefficients reducing significantly the efficiency of the method compared to its time-domain couterpart.

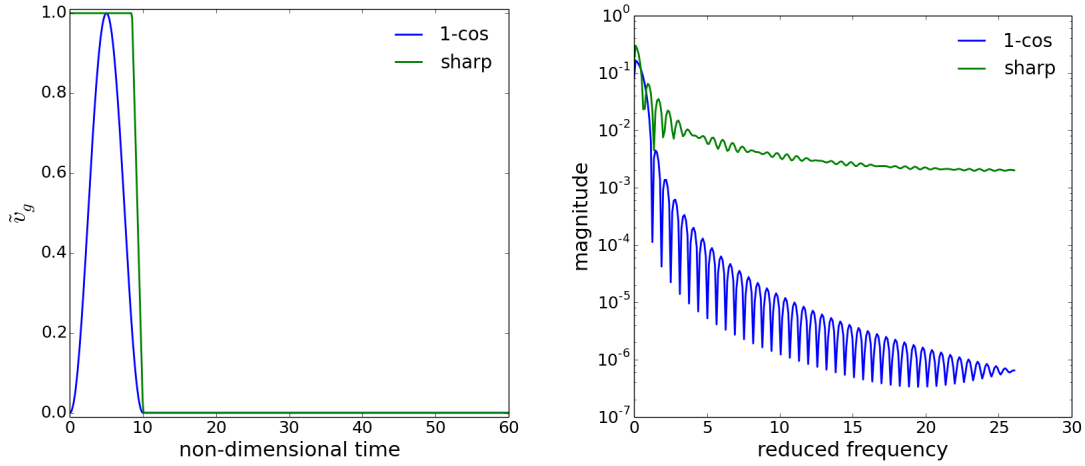

(a) time-domain (b) frequency-domain

Figure 1: Time- and frequency-domain signals of 1-cos ($L_g = 10\,\mathrm{m}$) and sharp-edged gust

2.2 Computational Fluid Dynamics Solver

The generation of snapshots to obtain the POD basis as well as the computation of the full-order reference solution is done with an in-house, semi-meshless Navier-Stokes flow solver [14, 15] coupled with the Spalart-Allmaras turbulence model [16]. Convective fluxes are discretised using upwind schemes, specifically the Osher solver for the mean flow equations [17]. A weighted least squares procedure calculates the gradients of the flow variables, required for viscous fluxes as well as source terms in the turbulence model. The steady-state solution is obtained applying a fully implicit backward Euler method with local time-stepping, while additionally a second order dual-time stepping is utilised in unsteady time-domain simulations. Linear equations arising from the implicit time integration and from the full-order LFD system are solved throughout using a restarted generalised conjugate residual method preconditioned with an incomplete lower-upper factorisation [18].

3 Results

Results are presented for the NACA 0012 aerofoil using a computational domain discretised with about 30×10^3 points. The point distribution has a structured layer near the wall to ensure a sufficient boundary layer resolution, seen in Figure 2, while the farfield distance is set to 50 chord lengths. Comparisons are shown for three different flow conditions to demonstrate the capability of the ROM for a variety of problems including sub- (S1) and transonic (T1) cases and an additional case exhibiting a shock-induced flow separation (T2). Comparisons of the full order model with a frequency-domain ROM are presented for S1 and T1 in [12]. The Reynolds number based on the chord length is 10 million, while the remaining flow parameters are summarised in Table 1.

The steady pressure coefficients on the surface are shown in Figure 3(a). A recompression shock can be observed for the transonic test cases T1 and T2. The shock position of T2 with a higher angle of attack is more upstream than in case T1. Since the shock position in attached flow moves downstream with increasing angle of attack, this reverse shock motion indicates flow separation. In Figure 3(b) the corresponding non-dimensional x-

Table 1: Main flow parameters of three considered test cases

Case	Mach number	Angle of attack [deg.]
S1	0.3	0.0
T1	0.8	0.0
T2	0.8	0.0

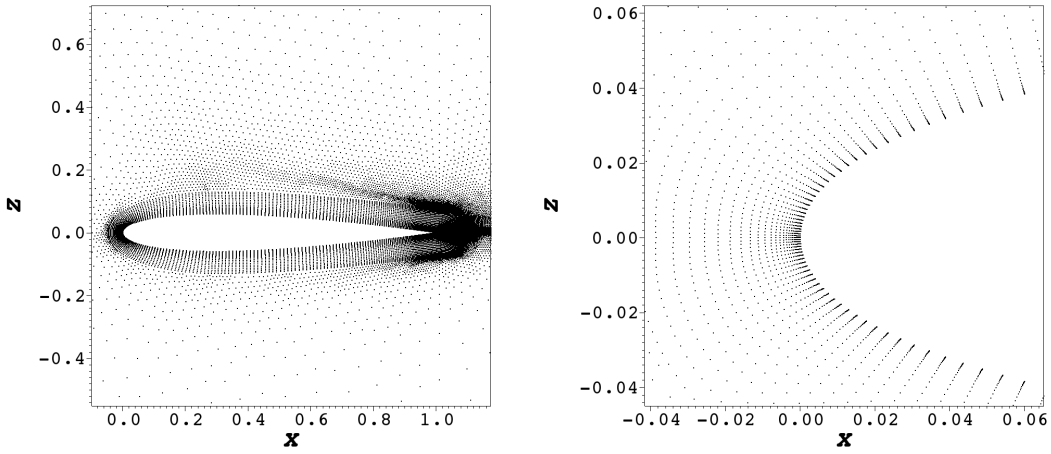

(a) computational domain (b) computational domain, zoomed-in

Figure 2: Computational domain of NACA 0012

velocity component is visualised. Besides the large supersonic zone, a region with negative velocities, as expected, can be observed behind the shock.

The ROM is generated using 40 snapshots of sinusoidal gust excitations computed at reduced frequencies in the interval $(0, 2\pi]$. The frequencies are distributed following the formula given in [12]:

$$\omega_k = \omega_0 + e^{-k\Delta\omega} \tag{8}$$

with suggested parameters $\omega_0 = 0.0$ and $\Delta\omega = 0.25\pi$. The responses to these sinusoidal gusts are computed with the LFD solver. The relative information content of the POD modes, i.e. the influence of each mode, and the dominant mode for case T2 are shown in Figure 4.

A drop of two orders of magnitude within the first 5 modes can be observed in Figure 4(a) for all test cases. A linear decrease until about the 50th mode can then be found for both attached-flow cases with a larger gradient in transonic flow. It is interesting to note, that the slope for the detached-flow case T2 shows a bump between the 10th and 15th mode and a linear decrease thereafter. This reflects a richer physical content close to the buffet onset. Since the ordinate is presented in logarithmic scale the linear decrease indicates the exponential decay of the relative information content. A criteria of $\sum_k r_k = 0.9999$ is used for the POD reduction throughout resulting in 29 basis vectors for case S1, 16 for T1 and 18 for T2.

For the detached-flow test case T2, the pressure's magnitude of the first POD mode, i.e. the mode with highest information content of $r_k = 0.955$, is displayed in Figure 4(b). In addition to the shock region, which is also present for the transonic attached-flow

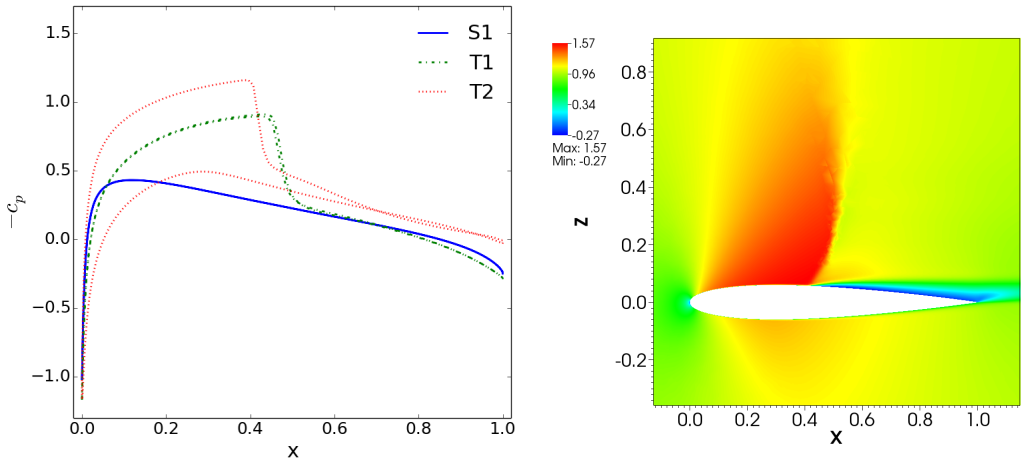

(a) surface pressure coefficients (b) x-velocity component for T2

Figure 3: Steady surface pressure coefficients for all cases and non-dimensional x-velocity for case T2

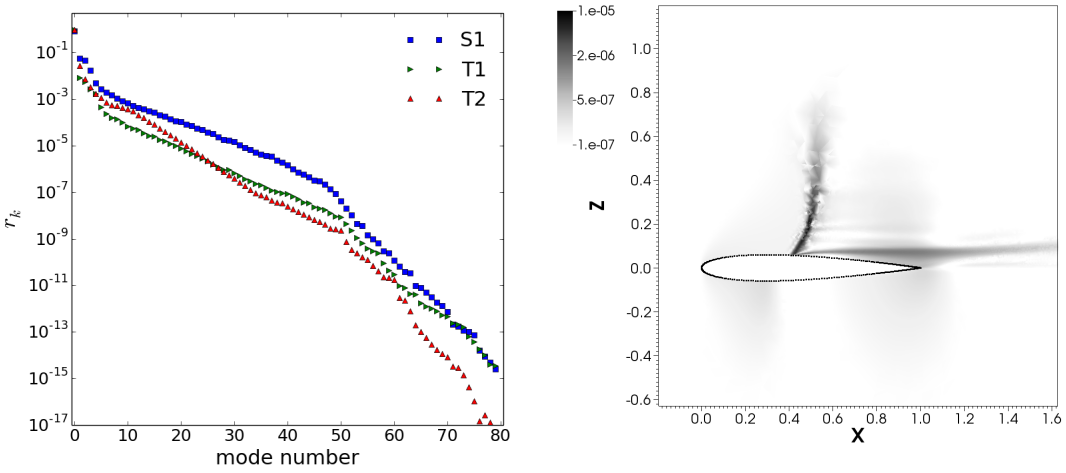

(a) relative information content (b) isobars of first POD mode for T2

Figure 4: Information content of POD modes and isobars of first POD mode for test case T2

case [12], high magnitudes can be observed around the free shear layer. If the shock is moving, the detached-flow topology changes as well explaining the similar magnitudes in both regions.

3.1 Responses due to 1-cos gusts

Comparisons of the lift response due to different 1-cos gusts are presented in Figure 5. The gust lengths are $L_g = 10\,\mathrm{m}$ and $L_g = 20\,\mathrm{m}$ with a reference point 10 m upstream of the aerofoil. The full order reference solutions (FOM) are computed using the non-linear time-domain solver with a non-dimensional time step of 0.02. For both cases with attached flow the non-dimensional gust amplitude $w_{g,z} = v_{g,z}/U_\infty = 10^{-2}$ is chosen throughout. Overall, good agreement can be found between the time-domain ROM and the full-order reference. For the subsonic case in Figure 5(a) the maximum is slightly overpredicted by the ROM because of amplitude non-linearities. The influence of the gust amplitude on

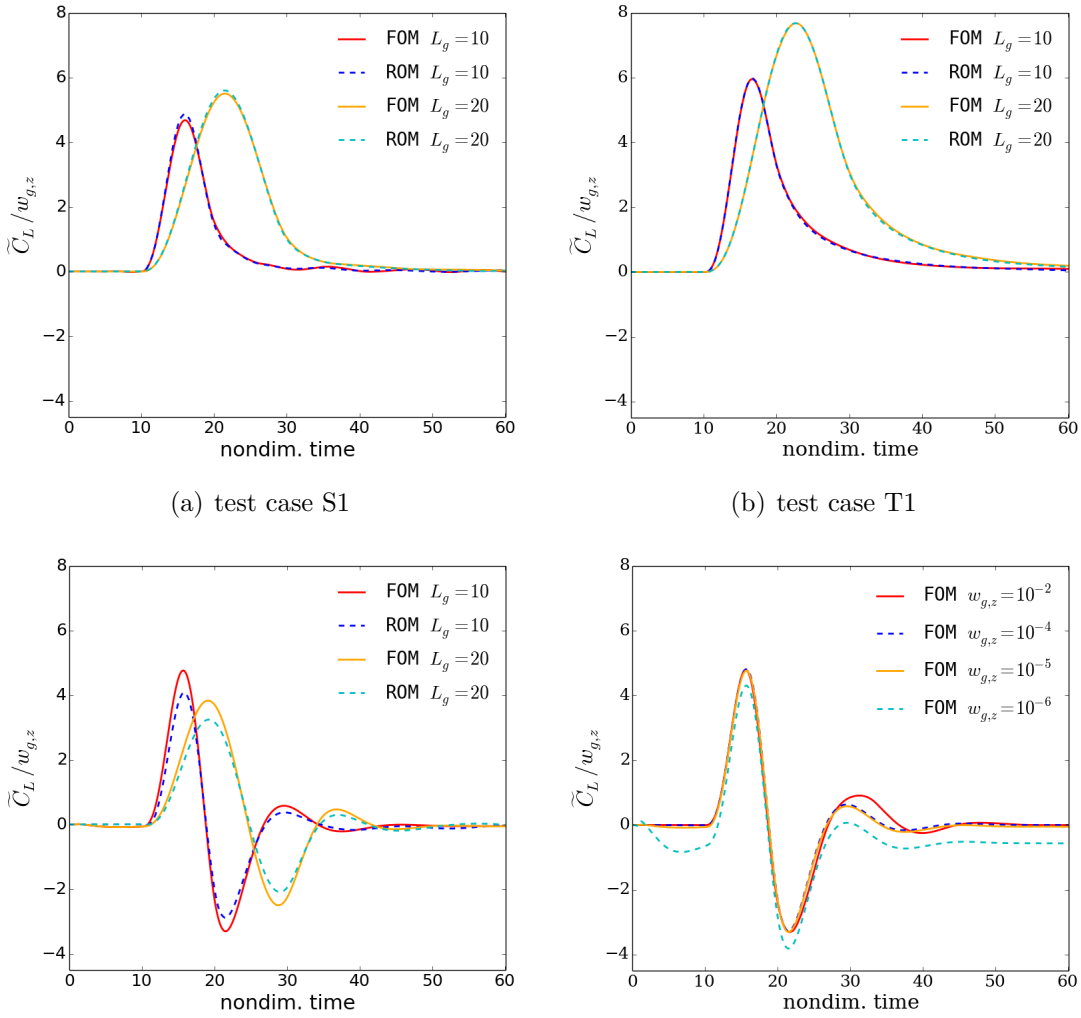

(a) test case S1

(b) test case T1

(c) test case T2

(d) test case T2 at $L_g = 10\,\mathrm{m}$

Figure 5: Change in lift coefficient due to different 1-cos gusts

the lift coefficient is presented in [12] showing a decrease in amplitude of the non-linear solution compared to a time-linearised solver. The agreement between both methods is better for the attached-flow transonic case T1. The maximum response in lift coefficient and the decay afterwards agree well.

The lift response changes significantly for case T2 with shock-induced separated flow as seen in Figure 5(c) and 5(d), exhibiting a distinct minimum following the global maximum. This indicates a large influence of an additional frequency, which is known from resonance peaks in frequency response functions close to buffet onset [19, 20]. Detached-flow cases are more sensitive concerning the excitation amplitude and its effect is thus analysed in Figure 5(d). While the global maximum in lift response is almost independent of the gust amplitude, the subsequent oscillations show a clear influence which diminishes for non-dimensional amplitudes $w_{g,z} \leq 10^{-4}$. At very small amplitudes with $w_{g,z} \leq 10^{-6}$, the solution of the RANS solver becomes inaccurate because of limited machine precision. In Figure 5(c) the results of the linear ROM are compared to non-linear responses with a gust amplitude of $w_{g,z} = 10^{-5}$. The reduced formulation is capable to reproduce the complex progression of the lift coefficient qualitatively, while underestimating its extrema.

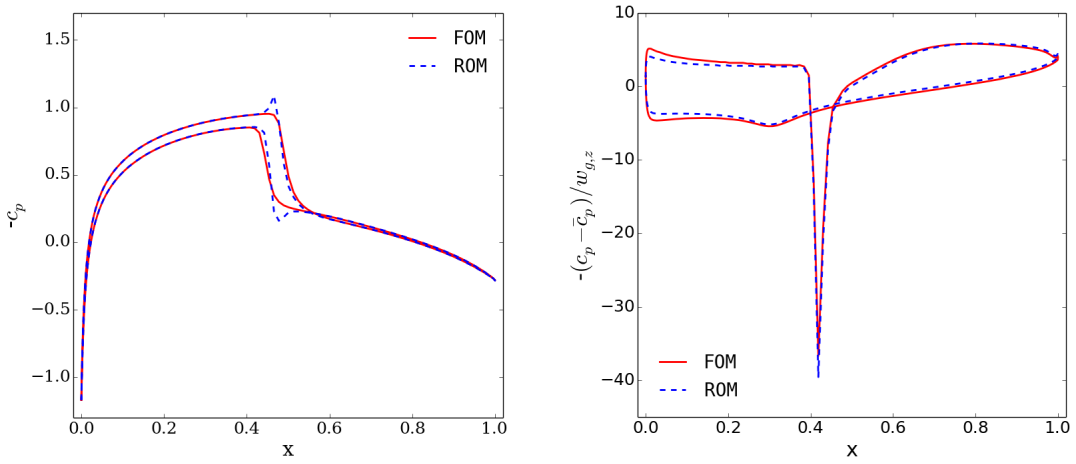

(a) test case T1 (b) test case T2

Figure 6: Surface pressure coefficients at maximum lift response for $L_g = 10\,\mathrm{m}$

In Figure 6, the instantaneous pressure coefficients are presented at the time step of the maximum lift response for both transonic test cases. For the attached-flow case T1 an amplitude was chosen yielding visual differences to the steady-state solution in Figure 3(a). Although amplitude effects can be observed at the shock location, the ROM prediction agrees well with the corresponding full order solution. The values around the shock on both surfaces are overpredicted by the linear ROM, caused by the superposition of the steady-state solution and the POD modes with rather high amplitudes. A smaller gust amplitude is simulated for the detached-flow case T2 and a plot of instantaneous pressure coefficients would simply show the steady state. Thus, the normalised difference to the steady surface pressure coefficient

$$\widetilde{c}_p = \frac{c_p(t) - \bar{c}_p}{w_{g,z}}$$

is displayed in Figure 6(b) instead. Good agreement between both methods is obtained in the region of separated flow, while the ROM predicts a slightly larger shock peak and smaller pressure differences around the leading edge.

3.2 Responses due to sharp-edged gust

After simulating responses due to 1-cos gusts, the capabilities of the time-domain ROM are demonstrated for a gust shape not easily represented by a Fourier series with a finite number of coefficients. Contrary to a 1-cos gust, a sharp-edged gust excites also high frequencies, as shown in Figure 1(b). The Fourier series cannot be truncated which contradicts the application of a ROM in frequency-domain.

Responses to a smoothed sharp-edged gust with a non-dimensional gust amplitude of 10^{-3} are computed for the three test cases. The step in gust velocity was smoothed with a linear increase over 1.5 chord length, shown as dotted black line in Figure 7(a), to improve convergence of the full order model. Results for the same gust shape are then calculated by the ROM using the same POD basis as for the 1-cos responses. For both attached-flow cases, the response in lift coefficients shows qualitatively the same progression as the Küssner function [21]. Excellent agreement can be found between results computed

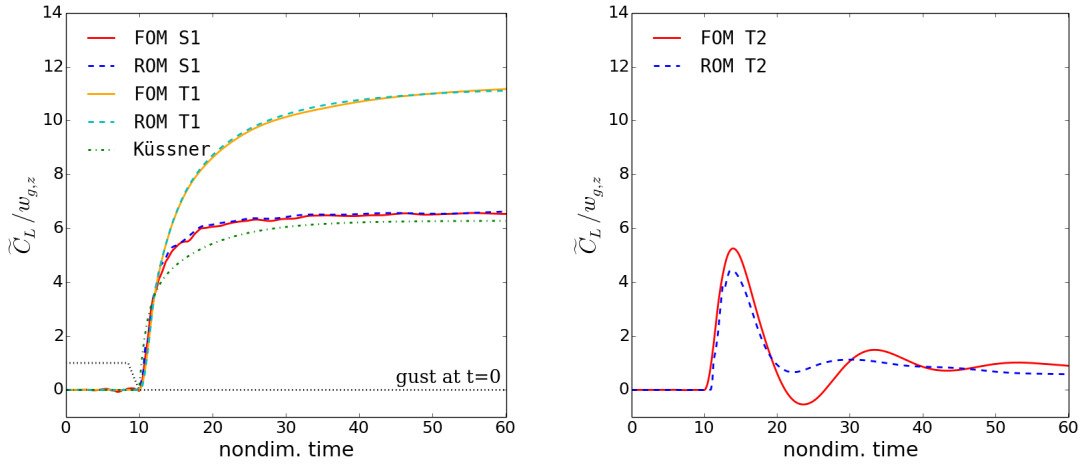

(a) attached-flow cases S1 and T1

(b) detached-flow case T2

Figure 7: Change in lift coefficient due to smoothed sharp-edged gust with $w_{g,z} = 10^{-3}$

by the ROM and the full order model. The response of the subsonic case obtained by the non-linear flow solver shows minor oscillations which are filtered by the ROM. The corresponding lift coefficient for the detached-flow case T2, shown in Figure 7(b), differs significantly exhibiting a maximum and damped oscillations thereafter. This distinct behaviour can be explained by looking at frequency responses due to pitch motion as presented in [19, 20] for constant Mach number and increasing angle of attack.

At attached-flow conditions the lift response is similar to predictions by linear potential theory such as Theodorson [22] starting with a large value at zero frequency and decreasing monotonically thereafter. However, close to shock buffet onset the quasi-steady derivative is decreasing significantly, which is the reason for the reduced lift gain after the sharp-edged gust passed the aerofoil. Moreover, the frequency response function exhibits a local maximum at the buffet frequency where an eigenvalue of the fluid Jacobian matrix is weakly damped causing the oscillations in Figure 7(b). The ROM predicts a maximum at the same time step, but at a smaller value and the lift coefficient oscillates at much smaller amplitude.

4 Conclusion

The paper describes a time-domain reduced order model based on proper orthogonal decomposition for gust response analysis. The reduced order model is trained by responses due to sinusoidal gusts computed with a linear frequency-domain solver. The linearised Reynolds-averaged Navier-Stokes equations are projected onto the subspace yielding a small-sized ordinary differential equation for the modal coefficients, subsequently used to reconstruct the physical solution from the projection basis. Different disturbances such as 1-cos or sharp-edged gusts can then be predicted at low cost.

Results are presented for the NACA 0012 aerofoil at three different flow conditions covering sub- and transonic flow without boundary layer separation and a shock-induced, separated flow. Lift responses of 1-cos gusts with two different wave lengths show an excellent agreement between the reduced order model and the non-linear, time-domain full order reference solution for the attached-flow cases. Only a minor difference can be observed in the subsonic case with the linear reduced order model overpredicting the max-

imal lift response due to amplitude non-linearities in the full order model. A comparable good agreement is obtained for the instantaneous surface pressures showing only small differences around the shock location for the transonic case. The lift responses due to a sharp edged gust give a progression similar to the Küssner function for both attached-flow cases demonstrating a good agreement between the considered methods. The lift response for the test case with shock-induced separation however changes significantly showing additional oscillations for both gust shapes due to the proximity to an inherent flow instability. The reduced order model can predict these features qualitatively, while underestimating amplitudes.

Future work will extend the presented methods to include additional Taylor coefficients to account for amplitude non-linearities. Moreover, the reduced order model will also be coupled with a controller for gust load alleviation.

5 Acknowledgement

This project has received funding from the European Union's Horizon 2020 research and innovation programme under grant agreement No 636053.

REFERENCES

[1] Dimitrov, D. and Thormann, R., "DLM-Correction Methods for Aerodynamic Gust Response Prediction," *International Forum on Aeroelasticity and Structural Dynamics*, 2013, IFASD 2013-24C.

[2] Wales, C., Jones, D., and Gaitonde, A., "Prescribed Velocity Method for Simulation of Aerofoil Gust Responses," *Journal of Aircraft*, Vol. 52, No. 1, 2015, pp. 64–76.

[3] Raveh, D. E., "CFD-Based Models of Aerodynamic Gust Response," *Journal of Aircraft*, Vol. 44, No. 3, 2007, pp. 888–897.

[4] Reimer, L., Ritter, M., Heinrich, R., and Krüger, W., "CFD-based Gust Load Analysis for a Free-flying Flexible Passenger Aircraft in Comparison to a DLM-based Approach," *22nd AIAA Computational Fluid Dynamics Conference*, 2015, AIAA 2015-2455.

[5] Wales, C., Gaitonde, A., and Jones, D., "Reduced order modelling for aeroelastic aerofoil response to a gust," *51st AIAA Aerospace Sciences Meeting including the New Horizons Forum and Aerospace Exposition*, 2013, AIAA 2013-0790.

[6] Dowell, E. H., Hall, K. C., Thomas, J. P., Kielb, R. E., Spiker, M. A., Li, A., and Denegri, Jr., C. M., "Reduced Order Models in Unsteady Aerodynamic Models, Aeroelasticity and Molecular Dynamics," *ICAS - 26th Congress of International Council of the Aeronautical Sciences*, 2008, ICAS 2008-0.1.

[7] Lumley, J. L., *The Structures of Inhomogeneous Turbulent Flow*, Atmospheric Turbulence and Radio Wave Propagation, 1965.

[8] Kim, T., "Frequency-Domain Karhunen-Loève Method and Its Application to Linear Dynamic Systems," *AIAA Journal*, Vol. 36, No. 11, 1998, pp. 2117–2123.

[9] Thormann, R. and Widhalm, M., "Linear-Frequency-Domain Predictions of Dynamic-Response Data for Viscous Transonic Flows," *AIAA Journal*, Vol. 51, No. 11, 2013, pp. 2540–2557.

[10] Hall, K. C., Thomas, J. P., and Dowell, E. H., "Proper Orthogonal Decomposition Technique for Transonic Unsteady Aerodynamic Flows," *AIAA Journal*, Vol. 38, No. 10, 2000, pp. 1853–1862.

[11] Thomas, J. P., Dowell, E. H., and Hall, K. C., "Three-Dimensional Transonic Aeroelasticity Using Proper Orthogonal Decomposition-Base Reduced-Order Models," *Journal of Aircraft*, Vol. 40, No. 3, 2003, pp. 544–551.

[12] Bekemeyer, P. and Timme, S., "Reduced Order Gust Response Simulation using Computational Fluid Dynamics," *57th AIAA/ASCE/AHS/ASC Structures, Structural Dynamics, and Materials Conference, AIAA SciTech*, 2016, AIAA 2016-1485.

[13] Parameswaran, V. and Baeder, J. D., "Indicial aerodynamics in compressible flow-direct computational fluid dynamic calculations," *Journal of Aircraft*, Vol. 34, No. 1, 1997, pp. 131–133.

[14] Kennett, D. J., Timme, S., Angulo, J., and Badcock, K. J., "An Implicit Meshless Method for Application in Computational Fluid Dynamics," *International Journal for Numerical Methods in Fluids*, Vol. 71, No. 8, 2013, pp. 1007–1028.

[15] Kennett, D. J., Timme, S., Angulo, J., and Badcock, K. J., "Semi-Meshless Stencil Selection for Anisotropic Point Distributions," *International Journal of Computational Fluid Dynamics*, Vol. 26, No. 9-10, 2012, pp. 463–487.

[16] Spalart, P. R. and Allmaras, S. R., "A One-Equation Turbulence Model for Aerodynamic Flows," *Recherche Aerospatiale*, Vol. 1, 1994, pp. 5–21.

[17] Osher, S. and Solomon, F., "Upwind Difference Schemes for Hyperbolic Systems of Conservation Laws," *Mathematics of Computation*, Vol. 38, 1982, pp. 339–374.

[18] Saad, Y., *Iterative Methods for Sparse Linear Systems*, Society for Industrial and Applied Mathematics, Philadelphia, PA, 2nd ed., 2003.

[19] Nitzsche, J., "A Numerical Study on Aerodynamic Resonance in Transonic Separated Flow," *International Forum on Aeroelasticity and Structural Dynamics*, June 2009, IFASD-2009-126.

[20] Thormann, R., Nitzsche, J., and Widhalm, M., "Time-linearized Simulation of Unsteady Transonic Flows with Shock-Induced Separation," *European Congress on Computational Methods in Applied Sciences and Engineering*, 2012, ECCOMAS 2012.

[21] Küssner, H. G., "Zusammenfassender Bericht über den instationären Auftrieb von Flügeln," *Luftfahrtforschung*, Vol. 13, No. 2, 1936, pp. 410–424.

[22] Theodorsen, T., "General Theory of Aerodynamic Instability and the Mechanism of Flutter," *NACA Report*, , No. 496, 1935, pp. 413–433.